Thermodynamic modeling and energy analysis of a polyamine-based water-lean solvent for CO_2 capture

Wonho Jung, Myungsuk Lee, Gyeong S. Hwang, Eunseok Kim, Kwang Soon Lee

PII: S1385-8947(20)31842-8
DOI: https://doi.org/10.1016/j.cej.2020.125714
Reference: CEJ 125714

To appear in: *Chemical Engineering Journal*

Received Date: 6 March 2020
Revised Date: 28 May 2020
Accepted Date: 29 May 2020

Please cite this article as: W. Jung, M. Lee, G.S. Hwang, E. Kim, K. Soon Lee, Thermodynamic modeling and energy analysis of a polyamine-based water-lean solvent for CO_2 capture, *Chemical Engineering Journal* (2020), doi: https://doi.org/10.1016/j.cej.2020.125714

Thermodynamic modeling and energy analysis of a polyamine-based water-lean solvent for CO_2 capture

Wonho Jung[a], Myungsuk Lee[b], Gyeong S. Hwang[b], Eunseok Kim[a], Kwang Soon Lee[a*]

[a]*Depart. of Chemical and Biomolecular Engineering, Sogang University, 35 Baekbeom-ro, Mapo-gu, Seoul 04107, Korea*

[b]*Depart. of Chemical Engineering, University of Texas at Austin, Austin, TX 78712, USA*

*Corresponding author. Tel.:+82-2-705-8477, e-mail: kslee@sogang.ac.kr

Abstract

Amine-based water-lean solvents are considered to be promising energy-saving alternatives to existing aqueous amine solvents for CO_2 capture. Herein, we propose water-lean solvents comprising 3,3'-iminobis(*N*,*N*-dimethylpropylamine) (60 wt%), water (10–18 wt%), and a non-amine chemical (balance), probe the solubility of CO_2 therein, and perform the energy demand analysis using an Aspen Plus®-based simulator. For CO_2 solubility modeling, the e-NRTL model and Redlich-Kwong state equation were incorporated with the equilibrium reaction model proposed by previous researchers, and the Henry's law constant of CO_2 was estimated using molecular dynamics simulation as it is difficult to measure experimentally. Experimental data acquired using an equilibrium cell and $^{13}C/^{1}H$ NMR were used to regress the equilibrium reaction model. The minimum thermal energy demand under desorber pressures of 303 and 505 kPa was calculated to be as low as 1.99 and 1.95 GJ t-CO_2^{-1}, respectively, which supports the suitability of the developed WLSs for post-combustion CO_2 capture.

Keywords: CO_2 capture; Water-lean solvent; Thermodynamic model; Energy evaluation

1. Introduction

According to most integrated assessment models [1,2], CO_2 capture and storage (CCS) has to play a key role to limit the warming to less than 2°C over the entire period up to 2100 [3]. Various CO_2 capture technologies to remove CO_2 from large-scale emission sources have been extensively researched for more than past two decades [4-7], and amine scrubbing is generally agreed to be closest to commercial deployment for now among various alternative technologies such as adsorption, membrane, chemical looping, and so forth. To date, progress in amine scrubbing technology allows one to lower the cost of CO_2 capture and construct/operate large CO_2 capture plants capable of producing 3,000 to 5,000 t-CO_2 day^{-1} for use in enhanced oil recovery [3,8]; however, the cost of CO_2 capture must be further decreased for this technology to become more widespread. In view of the widely held opinion that traditional aqueous amine-based absorption technology has reached its limit and can no longer be improved, the water-lean solvent (WLS) approach has drawn new attention, as it allows the solvent regeneration energy to be decreased by reducing water evaporation in the reboiler [9].

Many studies on WLSs have been performed on a laboratory scale, whereas only a few studies deal with the stage of pilot plant testing [9,10]. Barzagli *et al.* [11] exploited a WLS comprising 2-amino-2-methyl-1-propanol, piperazine, ethylene glycol monoethyl ether, and water, revealing that this solvent features a specific heat capacity (2.5–2.7 kJ kg^{-1}

K^{-1}) lower than that of the conventional aqueous solvent and can be regenerated at significantly lower temperatures (80–90 °C) and atmospheric pressure. Mathias *et al*. [12,13] proposed CO_2-binding organic liquids (CO_2BOLs) with an energy demand 33% lower than that of 30 wt% monoethanol-amine (MEA). However, the viscosity of such CO_2BOLs, which contain 1-(1,3-dimethylimidazolidin-2-ylidene)aminopropan-2-ol as the major amine, increases to 3000 cP upon full CO_2 loading, and continuous research on viscosity reduction is therefore under way. RTI International developed non-aqueous amine solvents that comprise hydrophobic, sterically hindered, carbamate-forming amines [14], have low regeneration temperatures of approximately 363 K, allow the use of low-pressure steam or waste heat, and feature absorption heats of 75 and 55–70 kJ mol^{-1} at 313 and 363 K, respectively. When these solvents were tested in a 485 SLPM-scale pilot process, a thermal energy demand of 2.3 GJ t-CO_2^{-1} was realized, which is around 65% of the value achieved in the commercial MEA-30 wt%-based process.

The solvents surveyed above contain no or small amounts of water, and their thermophysical properties are therefore strongly influenced by the major amine component. On the other hand, most aqueous amine solvents contain water at a mole fraction of larger than 0.8, and many of their properties are therefore dominated by those of water.

Herein, we investigated the characteristics of a novel polyamine-based WLS containing 60 wt% of 3,3'-iminobis(*N*,*N*-dimethylpropylamine) or IBDMPA, 10–18 wt% of water, and 22–30 wt% of a non-amine chemical (NAC; added to increase the thermal stability and CO_2 absorption rate of the solvent, identity not disclosed for confidentiality reasons). The solubility of CO_2 in the developed WLSs was measured using an equilibrium cell (EC), and liquid-phase speciation was probed by $^1H/^{13}C$ NMR measurements. The acquired data were used to regress an equilibrium reaction model proposed by Na *et al*. [15]. The e-NRTL model was employed to represent the activity coefficient, and the Redlich-Kwong equation of state was used to calculate vapor fugacity coefficients. The Henry's law constant of CO_2 in the WLS was estimated by molecular dynamics (MD) simulation, as they were hard to obtain experimentally. Finally, solvent regeneration energy was calculated using an Aspen Plus®-based process simulator for the standard absorber-desorber configuration except for inter-stage cooling in the absorber. Hereafter, IBDMPA will be denoted as IBD for simplicity of presentation if there is no confusion.

2. Solvent description

2.1. IBD and equilibrium reactions

IBD (M_w = 187.33 Da, bp = 239.4 °C at 101 kPa) is a polyamine possessing tertiary amine groups at both ends of its molecular backbone and a secondary amine group at its center (Fig. 1).

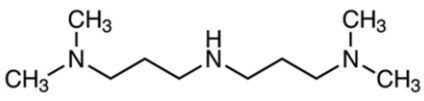

Fig. 1. Structure of IBD.

Na *et al*. [15] explored the species present in the IBD-CO_2-H_2O system by $^1H/^{13}C$ NMR measurements at IBD contents of 9.37–37.5 wt% and proposed a CO_2 solubility model described by the following equilibrium reactions:

Dissociation of water

$$2H_2O \overset{K_{eq,1}}{\leftrightarrow} OH^- + H_3O^+ . \quad (1)$$

Bicarbonate formation

$$CO_2 + 2H_2O \overset{K_{eq,2}}{\leftrightarrow} H_3O^+ + HCO_3^- . \quad (2)$$

Dissociation of bicarbonate

$$H_2O + HCO_3^- \overset{K_{eq,3}}{\leftrightarrow} H_3O^+ + CO_3^{2-} . \quad (3)$$

Dissociation of protonated amines

$$IBDH^+ + H_2O \overset{K_{eq,4}}{\leftrightarrow} IBD + H_3O^+ . \quad (4)$$

$$IBDH_2^+ + H_2O \overset{K_{eq,5}}{\leftrightarrow} IBDH^+ + H_3O^+ . \quad (5)$$

$$IBDH_3^+ + H_2O \overset{K_{eq,6}}{\leftrightarrow} IBDH_2^+ + H_3O^+ . \quad (6)$$

Dissociation of protonated carbamates

$$H^+IBDCOO^- + H_2O \overset{K_{eq,7}}{\leftrightarrow} IBDCOO^- + H_3O^+ . \quad (7)$$

$$H_2^{2+}IBDCOO^- + H_2O \overset{K_{eq,8}}{\leftrightarrow} H^+IBDCOO^- + H_3O^+ . \quad (8)$$

Formation of carbamate

$$IBD + CO_2 + H_2O \overset{K_{eq,9}}{\leftrightarrow} IBDCOO^- + H_3O^+ . \quad (9)$$

In these equations, $K_{eq,i}$ represents the equilibrium constant of the i^{th} reaction. Na *et al*. [15] estimated the above equilibrium constants under the assumption that the Henry's law constant of CO_2 is equal to that of the MEA-30 wt% solvent, which has previously been reported. This assumption is reasonable, as the mole fraction of water in both IBD-based and MEA-30 wt% solvents is greater than 0.85. However, the assumption is not valid for WLSs because of their far lower water content.

2.2. Solution state of the IBD-based WLS

The effects of water content on CO_2 solubility were probed by examining solvents with IBD : NAC : water weight ratios of 60 : 30 : 10 (WLS1), 60 : 27 : 13 (WLS2), and 60 : 22 : 18 (WLS3), respectively.

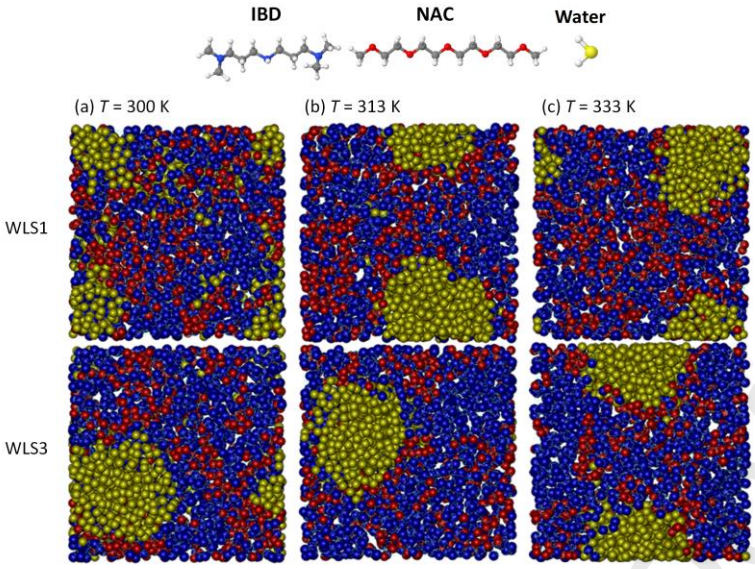

Fig. 2. MD snapshots of WLSs. IBD, NAC, and water are represented by blue, red, and yellow spheres, respectively.

MD simulations were performed using the GROMACS package to obtain the molecular-level solution states of WLS1 and WLS3 at three temperatures (Fig. 2) [16]. The optimized potentials for liquid simulations-all atom force field [17,18] was employed for IBD and NAC with the SPC/E water model [19] and a flexible version of the EPM2 force field was employed for CO_2 [20,21]. Lennard-Jones and Coulomb interactions were computed with a spherical cutoff of 10^{-9} m, while long-range electrostatic interactions were accounted for using the particle mesh Ewald summation method. Simulations were implemented in the NVT ensemble with the temperature controlled by a Nose-Hoover thermostat [22]. The initial systems were annealed at 1000 K within the NVT ensemble, compressed to the appropriate density, further annealed at 1000 K, and quenched to 300 K. For system equilibration, the additional NVT run was conducted at 300 K for 2 ns. To determine solution states at the elevated temperature, the equilibrated states at 300 K were run within the NPT ensemble at 313 and 333 K, which was followed by 2-ns NVT runs.

In Fig. 2, NAC and IBD molecules are well mixed and dispersed, while water molecules are clustered. Although IBD molecules are directly bonded to water molecules in some places, NAC molecules link the cluster phase of water molecules to the disperse phase of IBD and NAC.

3. Experimental

All chemicals used for CO_2 solubility measurements and NMR analysis, including IBD (>98%), D_2O (>99 atom% D), and 1,4-dioxane (>99%), were purchased from Sigma Aldrich. CO_2 gas (99.999 vol%) was purchased from Dongwoo Gastech Co., Korea.

3.1. CO_2 solubility

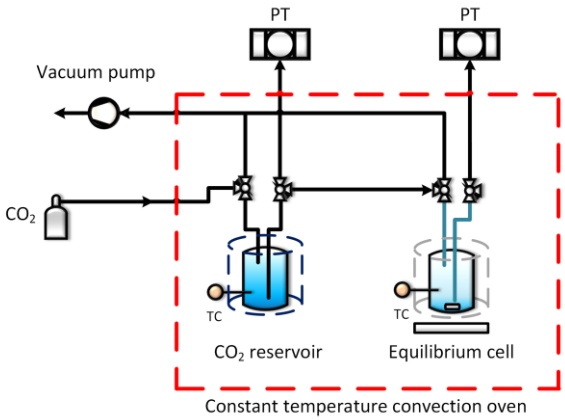

Fig. 3. EC unit for CO_2 solubility measurements.

CO_2 solubility was measured using the EC unit shown in Fig. 3. The CO_2 reservoir (2,000 mL) and EC (340 mL) were placed in a constant-temperature convection oven. The EC was charged with the solvent (70 mL) and evacuated until the vessel pressure reached the equilibrium partial pressure of water in the solvent, which is approximately 4 kPa at 313 K for WLS1 (10 wt% water). When this equilibrium pressure was reached, subsequent variation of vessel pressure becomes very slow. Then, the CO_2 reservoir was completely evacuated and filled with CO_2 up to approximately 707 kPa, and a part of CO_2 was transported to the EC. The equilibrium amount of CO_2 absorbed by the solvent was calculated from the amount of CO_2 lost in the CO_2 reservoir and the pressure of CO_2 in the EC. More details on the EC system and the calculation procedure are described in the work of Hwang *et al*. [23].

3.2. $^{1}H/^{13}C$ NMR measurements

^{1}H and ^{13}C NMR spectroscopic techniques were employed to analyze the speciation of the liquid phase as a function of CO_2 loading. Spectra were recorded on a 400-MHz Bruker instrument at 298 K up to a CO_2 loading of 0.8 mol-CO_2 mol-amine^{-1}. ^{1}H NMR was used only to detect bicarbonate formation. In the case of ^{13}C NMR, the delay time was approximately 5 s, and the number of scans was 1,000; 1,4-dioxane was used as an internal standard. D_2O was added to stabilize the signal and as an internal standard for ^{1}H NMR.

3.3. Viscosity and heat capacity

As the CO_2 loading increased from 0 to 60 g-CO_2 kg-solvent^{-1}, WLS viscosity, measured at 313 K using a viscometer (LVDV-II+P, Brookfield Ltd.), increased from 6 to 42 cP, while WLS heat capacity was measured as 2.45 ± 0.05 kJ kg^{-1} K^{-1} at 303–343 K using an in-house-made calorimeter.

4. Mathematical model

4.1. CO_2 solubility

The e-NRTL model was employed to construct the activity model [24]. In this section, only major equations are introduced to define the key variables used in data regression. The equilibrium constant for the i^{th} reaction was defined as

$$K_{eq,r} = \prod_{i=1,\cdots,N} a_i^{\eta_i} = \prod_{i=1,\cdots,N} (c_i \gamma_i)^{\eta_i} , \tag{10}$$

where a [mol kg^{-1}], c [mol kg^{-1}], γ, and η represent the activity, molar concentration, activity coefficient, and stoichiometric coefficient, respectively, and subscript i refers to the i^{th} species. The temperature dependence of the equilibrium constant was modeled as [25]

$$\ln K_{eq,r} = A_{eq,r} + B_{eq,r} / T + C_{eq,r} \ln(T / [1\ \mathrm{K}]) + D_{eq,r} T , \tag{11}$$

where T [K] is temperature. The vapor-liquid equilibrium (VLE) model was expressed as

$$y_{\mathrm{CO_2}} \phi_{\mathrm{CO_2}} P = x_{\mathrm{CO_2}} \gamma_{\mathrm{CO_2}} (1 / H_{WLS}) \exp\left(\frac{\bar{v}_M^{\infty} (P - P_{\mathrm{H_2O}}^{sat})}{RT} \right), \tag{12}$$

where y, ϕ, P [Pa], x, γ, $\bar{v}_M^{\infty}$ and R [J mol^{-1} K^{-1}] are the gas molar fraction, fugacity coefficient, pressure, liquid molar fraction, activity coefficient, the partial molar volume of CO_2 in the solution at infinite dilution, and gas constant, respectively. H_{WLS} [mol m^{-3} Pa^{-1}] denotes the Henry's law constant of CO_2 in the WLS. The vapor fugacity coefficient was calculated using the Redlich-Kwong equation of state [26].

Liquid phase non-ideality was expressed using the e-NRTL activity coefficient model and excess Gibbs free energy, g^{ex*} [kJ mol^{-1}], with further details described in the work of Na *et al*. [15]. Local interactions were represented according to the NRTL theory. Based on the definition of local interactions, binary interaction parameters and non-randomness factors were used as adjustable parameters. The binary interaction parameter τ_{ij} can be expressed as

$$\tau_{ij} = \frac{U_{ij} - U_{jj}}{RT} = a_{ij} + \frac{b_{ij}}{T} , \tag{13}$$

where U_{ij} [kJ mol^{-1}] is the interaction energy between species i and j, each of which can be an ion or a molecule; a_{ij} and b_{ij} are fitting parameters, which, despite being generally dependent on temperature, were assumed to be constant to reduce model complexity.

4.2. Estimation of the Henry's law constant

The Henry's law constant (H), critically important to the CO_2-VLE model, is hard to obtain experimentally for the CO_2-solvent system because of the reaction of CO_2 in the solution. Hence, MD simulations were employed to calculate the H of CO_2 in the studied solvents. H is directly related to the free energy of solvation ($-\Delta_{sol}A$) as

$$H(T) = \frac{1}{RT}\exp\left(\frac{-\Delta_{sol}A}{RT}\right), \quad (14)$$

where $-\Delta_{sol}A$ [kJ mol^{-1}] is the solvation free energy. To calculate the $-\Delta_{sol}A$ of CO_2 for equilibrated solvents in section 2.2, we used the Bennett acceptance ratio (BAR) method [27], one of several free energy perturbation methods. The solvation path was described as thermodynamically reversible by creating a series of intermediate states as a function of coupling parameter λ. In our calculation, we applied a step of 0.05 from $\lambda = 0$ (completely decoupled) to $\lambda = 1$ (fully interacting) for the coupling of Coulombic and Lennard-Jones interactions between CO_2 and the solvent. For each λ, the production runs were implemented for 3 ns, and the free energy differences were then extracted from output data using the GROMACS BAR tool. Each calculation was repeated more than three times.

Temperature dependence of the Henry's constant can be alternatively described by the following van't Hoff equation [28]:

$$H(T) = H^0\exp\left(\frac{-\Delta_{sol}H}{R}\left(\frac{1}{T}-\frac{1}{T^o}\right)\right) \quad (15)$$

where $-\Delta_{sol}H$ [kJ mol^{-1}] is the solvation enthalpy, and superscript 0 refers to the reference state (T = 273 K). Equation (15) is used in the Aspen Plus® simulator.

4.3. Heat of absorption

The heat of absorption can be represented by the following Gibbs-Helmholtz equation [29]:

$$\left[\frac{\partial \ln P_{CO_2}}{\partial(1/T)}\right]_{\alpha_{CO_2}} = -\frac{\Delta H_{CO_2}}{R}, \quad (16)$$

where P_{CO2}, $-\Delta H_{CO2}$ [kJ mol^{-1}] and α_{CO2} [mol mol^{-1}] represent the equilibrium CO_2 partial pressure, heat of absorption, and CO_2 loading, respectively.

4.4. Data regression

From Eqs. (10)–(13), ($A_{eq,4}$, ⋯, $A_{eq,9}$, $B_{eq,4}$, ⋯, $B_{eq,9}$, $C_{eq,4}$, ⋯, $C_{eq,9}$, $D_{eq,4}$, ⋯, $D_{eq,9}$, a_{ij}, b_{ij}) were selected as fitting parameters for the binary interactions and equilibrium constants of the IBD-NAC-H_2O-CO_2 system. The Aspen Plus® regression tool was used to estimate the fitting parameters based on the following minimization criterion:

$$\min_{\theta} J = \sum_{k,i}\left[\left(\frac{P^{pre}_{CO_2,k}(\theta) - P^{exp}_{CO_2,k}}{\sigma_{P_{CO_2}}}\right)^2 + \left(\frac{x^{pre}_{i,k}(\theta) - x^{exp}_{i,k}}{\sigma_{x_i}}\right)^2\right], \quad (17)$$

$$\text{where } \theta = [A_{eq,4}\cdots A_{eq,9}\, B_{eq,4}\cdots B_{eq,9}\, C_{eq,4}\cdots C_{eq,9}\, D_{eq,4}\cdots D_{eq,9}\, a_{ij}\, b_{ij}]$$

where superscripts *pre* and *exp* represent model prediction and experimental measurement, respectively; σ is a normalization factor; and x_i denotes the mole fraction of species i in the liquid phase. For interaction parameter coefficients, all possible ij pairs were initially estimated. Insignificant pairs were then excluded through repeated sensitivity analysis, and 12 pairs were finally chosen and estimated.

5. Results and discussion

5.1. Henry's law constant

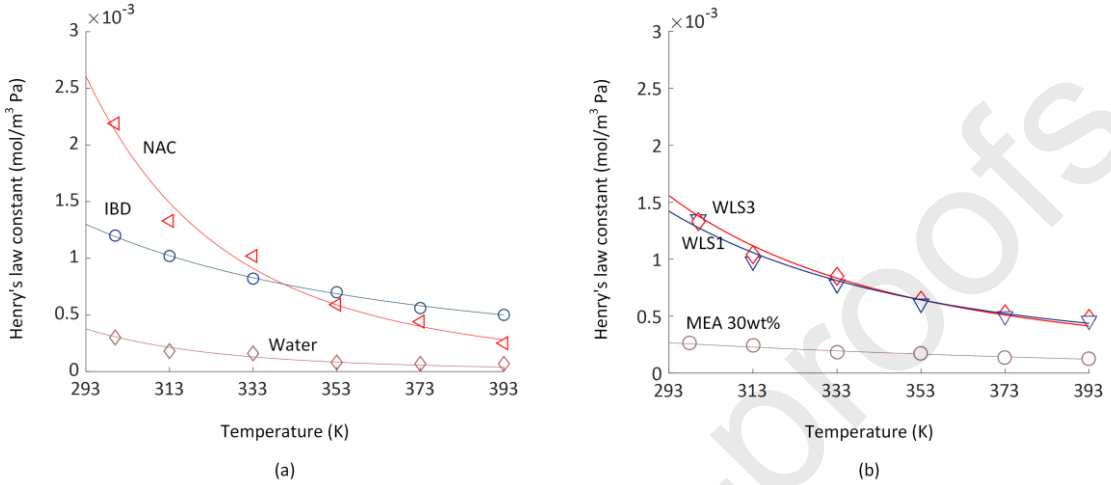

Fig. 4. Estimates of Henry's law constant of CO_2 in (a) each WLS component and (b) WLS1, WLS3, and MEA-30 wt%.

Table 1. Estimated Henry's law parameters.

Component	H^0 [mol m^{-3} Pa^{-1}]	$-\Delta_{sol}H$ [kJ mol^{-1}]
IBD/CO_2	17.13×10^{-4}	9.158
NAC/CO_2	22.39×10^{-4}	29.8
Water/CO_2	7.25×10^{-4}[a]	21.74[a]

[a]: reference [30].

Fig. 4(a) shows estimates of the temperature-dependent Henry's law constant of CO_2 (H) in each WLS component, with estimates of parameters contributing to H given in Table 1. Values of H in IBD and NAC at 290 K were estimated to be three and six times larger than H in water, respectively. This behavior was ascribed to the strong cohesion between water molecules induced by hydrogen bonding, which makes it difficult for CO_2 to infiltrate the water molecule network. On the other hand, IBD and NAC, as organic compounds, show weaker molecular cohesion than water, thus featuring larger Henry's law constants.

Fig 4(b) compares the temperature-dependent values of H in WLS1, WLS3, and MEA-30 wt%, showing that H in MEA-30 wt% behaves similarly to H in water, which was ascribed to the high mole fraction of water (0.89) in the MEA-30 wt% solvent. H's in WLS1 and WLS3 were similar and significantly exceeded H in MEA-30 wt%, decreasing with increasing temperature more rapidly than the H in MEA-30 wt%. It was assumed that H in WLS2 has the average of H values in WLS1 and WLS3.

5.2. CO_2 solubility

Figs. 5(a)–(c) display the results of CO_2 solubility measurements (through EC experiments) together with predictions

of the proposed solubility model for WLS1, WLS2, and WLS3, respectively. Fig. 5(d) is the redrawing of the model prediction for WLS1 obtained using *H* in MEA instead of the correct *H*. The model fit in Fig. 5(d) is worse than that in Fig. 5(a), which means that Henry's law constant is critical for the accurate modeling of CO_2 solubility in WLSs. Model predictions in Figs. 5(a)–(c) agree quite accurately with experimental data.

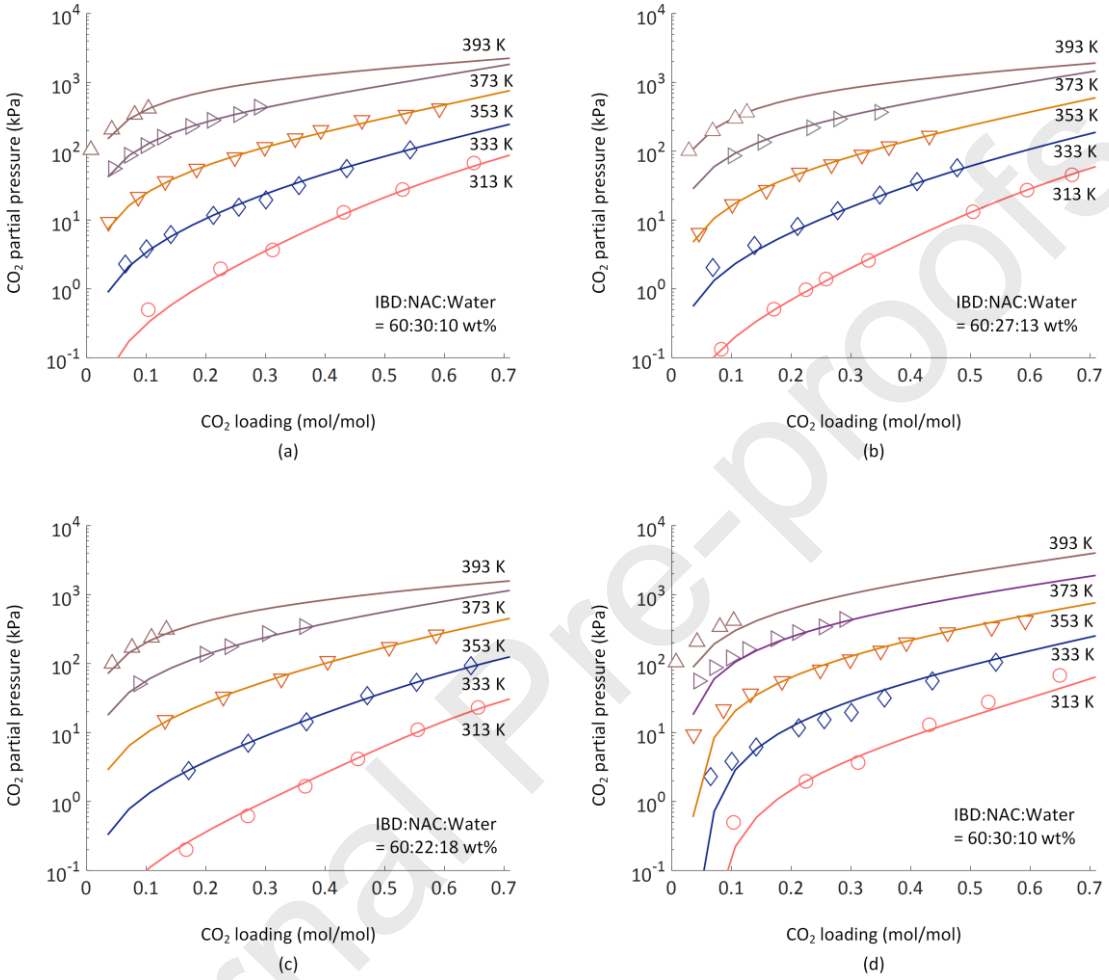

Fig. 5. EC data–based (dots) and model-predicted (solid lines) values of CO_2 solubility at 313, 333, 353, 373, and 393 K in (a) WLS1, (b) WLS2, (c) WLS3, and (d) WLS1 when *H* in MEA was used in the model.

Table 2. Estimated coefficients of selected binary interaction parameters.

i	*j*	Value		
		a_{ij}	b_{ij}	source
H_2O	CO_2	10.064	−3268.14	[31]
CO_2	H_2O	10.064	−3268.14	[31]
H_2O	IBD	11.1242	−3875.87	This work
IBD	H_2O	−11.0345	4514.3	This work
H_2O	$IBDH^+/HCO_3^-$	4.78394	–	This work
H_2O	$IBDH^+/CO_3^{2-}$	10	–	This work
$IBDH^+/CO_3^{2-}$	H_2O	−4	–	This work

H_2O	$IBDH^+/IBDCOO^-$	6.81489	–	This work
H_2O	$H_2^{2+}IBDCOO^-/HCO_3^-$	1.34155	–	This work
$H_2^{2+}IBDCOO^-/HCO_3^-$	H_2O	−2.7982	–	This work
H_2O	NAC	−61.8268	380.028	This work
NAC	H_2O	−66.8629	4828.73	This work

Table 3. Parameters estimates for reaction equilibrium constants.

Equation number	Equilibrium constant $K_{eq,r}$ (molality basis)				$K_{eq,i}$ (at 313 K)	Source
	$A_{eq,r}$	$B_{eq,r}$	$C_{eq,r}$	$D_{eq,r}$		
1	220.067	−12431.7	−35.4819	–	5.99×10^{-11}	[32]
2	235.482	−12092.1	−36.7816	–	5.02×10^{-7}	[32]
3	140.932	−13445.9	−22.4773	–	2.86×10^{-14}	[32]
4	66.6413	−28835.8	6.73729	−0.0944452	7.10×10^{-11}	This work
5	29.7846	−3682.46	–	–	1.49×10^{-8}	This work
6	34.7365	−25709.1	–	–	6.27×10^{-10}	This work
7	−49.2387	5470.86	–	–	1.99×10^{-12}	This work
8	25.4363	−12066.1	–	–	5.17×10^{-10}	This work
9	17.9003	8664.87	−10.5943	−0.0282689	8.67×10^{-10}	This work

Table 2 lists the estimated coefficients of binary interaction parameters in the e-NRTL model. The total number of undetermined binary interaction parameters equaled 88 and was reduced to 10 by repeated parameter estimation and sensitivity analysis. Table 3 shows estimates of the equilibrium reaction constant, $K_{eq,r}$, for nine reactions at 313 K. The reliability of parameter estimates was confirmed not only by the prediction of CO_2 solubility (Fig. 5), but also by the prediction of liquid-phase speciation (Fig. 8).

Effect of water content on the VLE curve. Fig. 5 reveals that the VLE curve shifts to the right with increasing WLS water content, in line with the concomitant shift of the equilibrium to the right according to Eqs. (1) and (9). For a fixed CO_2 loading, this means that the concentration of free CO_2 in the liquid phase and hence, the equilibrium CO_2 pressure in the gas phase, decreases.

Cyclic capacity. The cyclic CO_2 absorption capacity (or simply cyclic capacity) is defined as the difference between the rich and lean loadings and depends on operating conditions and process design. Herein, we considered the nominal cyclic capacity, defined by lean and rich loadings at equilibrium CO_2 partial pressures of 0.3 and 12 kPa, respectively. Frequently, the equilibrium CO_2 partial pressures for nominal lean and rich loadings are chosen as 0.1 and 5 kPa, respectively. The value of 12 kPa for the nominal rich loading was chosen because the CO_2 absorption rate of the IBD-based WLS is approximately three times faster (on average) than that of MEA-30 wt%. According to these definitions, MEA-30 wt% has a cyclic capacity of 0.2 mol mol^{-1} (~40 g-CO_2 kg-$solvent^{-1}$), whereas WLS1, WLS2, and WLS3 show 0.35, 0.36, and 0.40 mol-CO_2 mol-IBD^{-1} (50, 52, and 57 g-CO_2 kg-$solvent^{-1}$), respectively. Na *et al*. [15] has shown that an aqueous IBD solvent with 62.5 wt% water has a cyclic capacity of 0.56 mol-CO_2 mol-IBD^{-1} (~82 g-CO_2 kg-$solvent^{-1}$) (based on 0.1 and 5 kPa of the equilibrium CO_2 partial pressures for nominal lean and rich loadings), which suggests that an increase in amine content does not necessarily increase cyclic capacity.

Heat of absorption. In Fig. 5, the spacing between two adjacent isotherms decreases with increasing temperature for all

solvents, which, according to Eq. (15), means that $-\Delta H_{CO2}$ concomitantly decreases.

Fig. 6 shows the temperature dependence of $-\Delta H_{CO2}$ for the three WLSs and the MEA-30 wt% solution [33]. The profiles of $-\Delta H_{CO2}$ at 313 K over the CO_2 loading (Fig. 6(a)) represent the axial profiles of $-\Delta H_{CO2}$ inside a hypothetic isothermal absorber. Overall, $-\Delta H_{CO2}$ decreases with increasing CO_2 loading. This phenomenon is generally observed in other aqueous amine solvents, but was more pronounced in the studied WLSs. Fig. 6(b) shows profiles of $-\Delta H_{CO2}$ over a temperature range from 320 to 400 K for a CO_2 loading of 0.14 mol-CO_2 mol-IBD^{-1}, a typical lean loading value. In this sense, Fig. 6(b) can be regarded to represent the regeneration energy for reboiler temperatures of 320–400 K. Unlike for other aqueous amine solvents, $-\Delta H_{CO2}$ broadly varies with temperature. The investigated WLSs had large values of $-\Delta H_{CO2}$ in the low-temperature region but considerably smaller values at the reboiler temperature (coarsely above 375 K). At 390 K, the $-\Delta H_{CO2}$ of all three WLSs approximately equaled 50 kJ mol-CO_2^{-1}, i.e., 55% of the MEA-30 wt% value. This low $-\Delta H_{CO2}$ and small water evaporation in the reboiler suggest that our WLSs require much less regeneration energy than the MEA-30 wt% solvent.

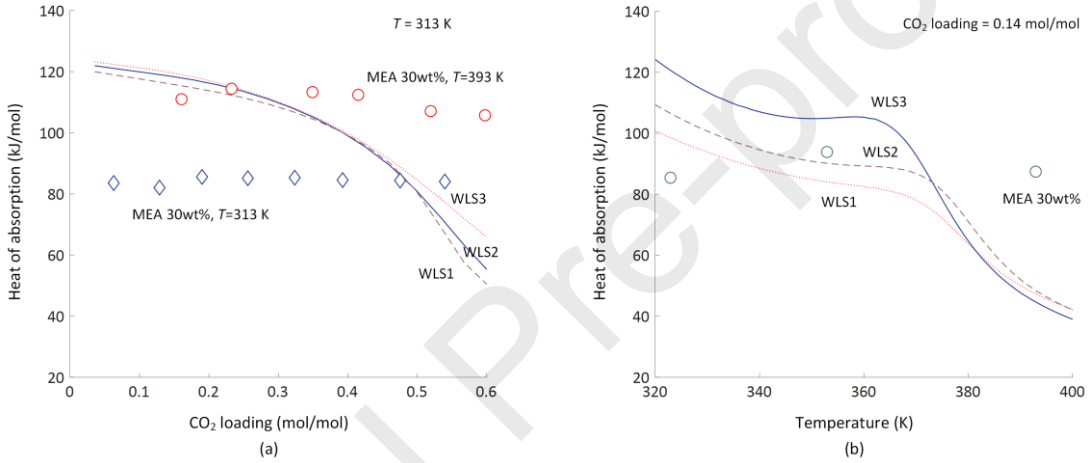

Fig. 6. Heat of absorption for WLS1–3 as a function of (a) CO_2 loading at 313 K and (b) temperature at a CO_2 loading of 0.14 mol-CO_2 mol-IBD^{-1}; Data for MEA 30wt% is from [33].

5.3. Speciation in solution

Fig. 7 represents the liquid phase speciation determined by ^{13}C NMR at 298 K for the three WLSs and the related model predictions. In ^{13}C NMR spectra, peaks of IBD and protonated IBD ($IBDH^+$, $IBDH_2^{2+}$, $IBDH_3^{3+}$) appeared at the same position. The same was true for $IBDCOO^-$ and protonated $IBDCOO^-$ ($H^+IBDCOO^-$, $H_2^{2+}IBDCOO^-$) as well as for HCO_3^- and CO_3^{2-}. The ^1H NMR peaks of HCO_3^- and CO_3^{2-} were distinct from each other but were not used for quantitative analysis because of the rather low measurement quality. Thus, ^1H NMR was only used to monitor bicarbonate ion formation. The NMR spectra of WLS1–3 for CO_2 loadings of 0.1, 0.3, 0.5, and 0.7 mol-CO_2 mol-IBD^{-1} are presented in Fig. S2. Overall, model predictions quite closely agreed with the results of NMR measurements, which verified the reliability of the developed equilibrium reaction model.

With increasing CO_2 loading, the mole fraction of water slightly decreased, that of IBD rapidly decreased, and the mole fraction of NAC remained constant. In the case of WLS1 (Fig. 7(a)), the contents of carbamate and protonated carbamate ions monotonically increased up to a CO_2 loading of 0.8 mol-CO_2 mol-IBD^{-1}, while bicarbonate and carbonate ions

(HCO_3^-/CO_3^{2-}) appeared at 0.4 mol-CO_2 mol-IBD^{-1} and became progressively more dominant with increasing CO_2 loading. Similar behavior was observed for aqueous MEA. On the other hand, the profiles of WLS2 and WLS3 (Figs. 7(b) and (c), respectively) show that HCO_3^-/CO_3^{2-} began to form at very low CO_2 loadings. The amounts of HCO_3^-/CO_3^{2-} in WLS2 and WLS 3 were larger than those in WLS1. Conversely, the amount of (protonated) $IBDCOO^-$ in WLS2 and WLS 3 was smaller than that in WLS1.

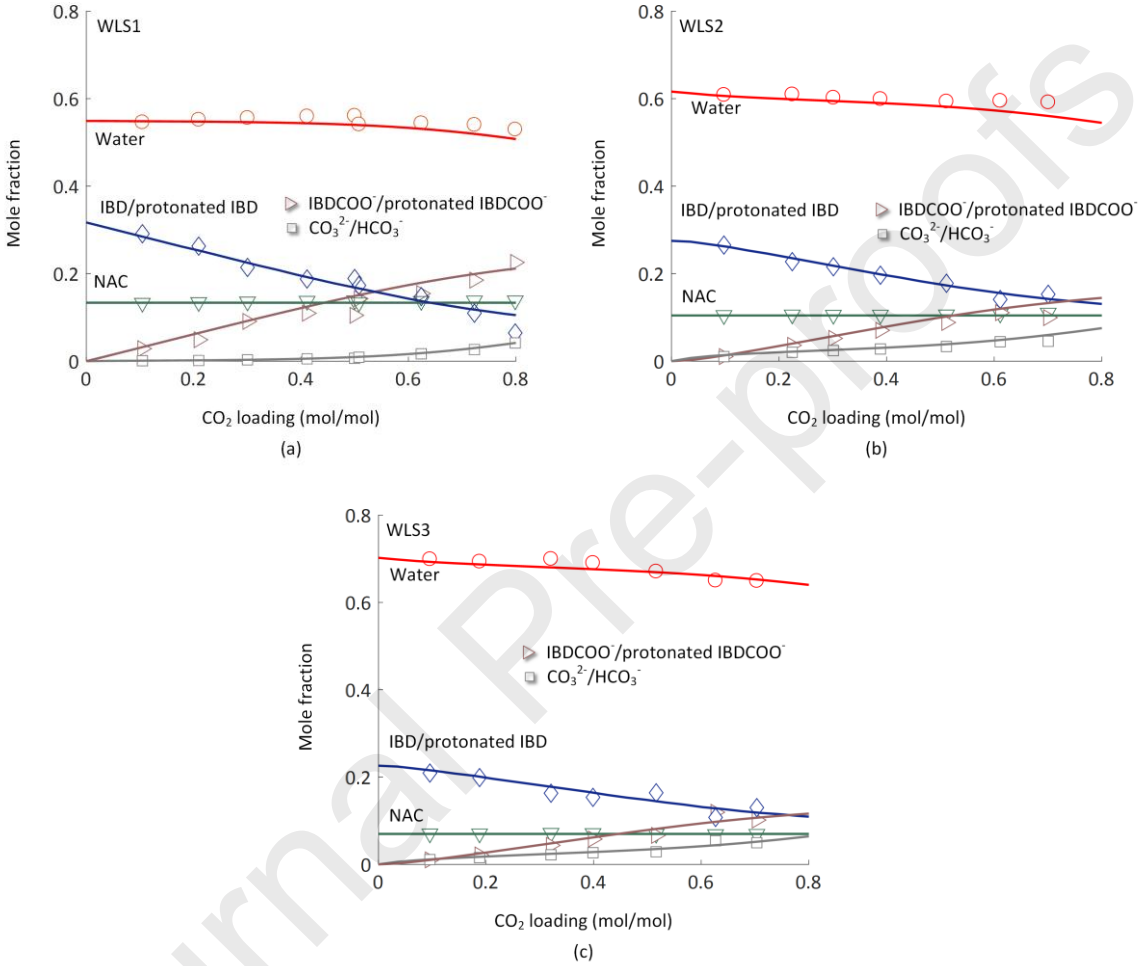

Fig. 7. Liquid phase speciation determined by ^{13}C NMR at 298 K (open symbols) and model predictions (solid lines) for (a) WLS1, (b) WLS2, and (c) WLS3.

Figs. 8(a)–(c) are extensions of Figs. 7(a)–(c), presenting model-calculated mole fraction profiles of all liquid-phase species at 313 K. The mole fractions of all species at lean and rich loadings are listed for the three WLSs in Table 4.

In the rich loading state, the free IBD to total IBD ratios of WLS1, WLS2, and WLS3 were determined as ~0.48. 0.42, and 0.34, respectively, i.e., the free IBD content decreased with increasing water content, while the mole fractions of protonated IBD were all close to 0.021. Carbamate ions largely existed in the zwitterionic form of $H^+IBDCOO^-$, but $IBDCOO^-$ and $H_2^{2+}IBDCOO^-$ were also present. The speciation of aqueous IBD (IBD : water = 30 : 70, w/w) determined by Na *et al.* [15] indicates that the $H_2^{2+}IBDCOO^-$ ion was rarely generated, while the overall trend was similar to that observed for WLS3. The bicarbonate concentration was smaller than the carbamate concentration over the whole operating

region of CO_2 loading, being positively correlated with water content and rapidly increasing beyond a certain CO_2 loading for all WLSs.

Notably, IBD content decreases faster in Fig. 8 than in Fig. 7, which indicates that the total ion concentration is higher in the former case. Thus, considering that Fig. 7 refers to a temperature of 298 K, while Fig. 8 refers to 313 K, we concluded that the reaction was promoted by high temperature.

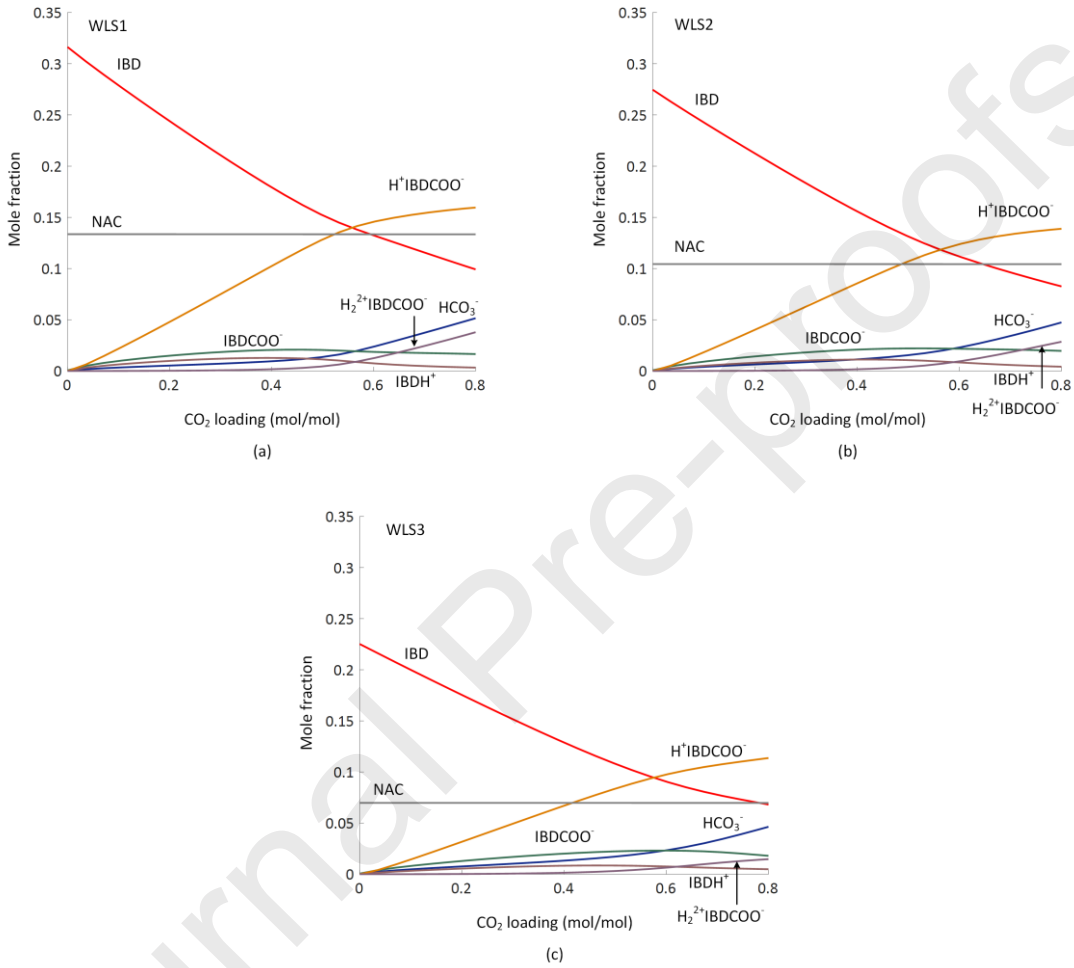

Fig. 8. Model-calculated profiles of all liquid-phase species at 313 K for (a) WLS1, (b) WLS2, and (c) WLS3. "Lean" and "Rich" are defined as nominal values corresponding to equilibrium CO_2 partial pressures of 0.3 and 12 kPa, respectively. The mole fractions of $IBDH_2^{2+}$ and CO_3^{2-} are too small to be shown.

Table 4. Mole fractions of liquid-phase species in WLSs for lean and rich loadings at 313 K.

	WLS1		WLS2		WLS3	
State	Lean	Rich	Lean	Rich	Lean	Rich
Loading	0.1 mol mol^{-1}	0.45 mol mol^{-1}	0.13 mol mol^{-1}	0.49 mol mol^{-1}	0.2 mol mol^{-1}	0.6 mol mol^{-1}
IBD	0.2766	0.1529	0.2192	0.1176	0.1471	0.0767
$IBDH^+$	0.0102	0.0206	0.0132	0.0219	0.0176	0.0215
$IBDCOO^-$	0.0067	0.0114	0.0075	0.0092	0.0075	0.0059

$H^+IBDCOO^-$	0.0234	0.1276	0.0352	0.1192	0.0529	0.1076
$H_2^{2+}IBDCOO^-$	–	0.0043	0.0002	0.0072	0.0007	0.0114
HCO_3^-	0.0035	0.0135	0.0059	0.0200	0.0108	0.0344

The levels of CO_3^{2-} and $IBDH_2^{2+}$ were negligible.

5.4. Thermal energy demand

WLSs have been studied with the aim to low reboiler heat duty by reducing water evaporation in the stripper reboiler. The IBD-based WLS described herein has the additional advantage of a high (compared to that of other amine solvents) equilibrium CO_2 pressure under reboiler conditions. For instance, the equilibrium CO_2 pressure of WLS1 at 393 K and 0.12 mol-CO_2 mol-IBD^{-1} is 475 kPa. Under these conditions, the partial pressure of water is 84 kPa, which indicates that a high stripper pressure of 555 kPa can be achieved at relatively low reboiler temperatures. Although the corresponding data are not shown here, the IBD-based WLS was found to be resistant to thermal degradation, which allows the stripper to be operated at even higher pressures. As discussed in Fig. 6, the small heat of the reaction at high temperatures can contribute to reboiler heat duty reduction. Finally, the small heat capacity provides an opportunity to lower sensible heat. On the contrary, the high viscosity (~40 cP at 313 K) at high rich loading decreases the heat transfer coefficient and thus increases the heat exchanger size.

The benefits of IBD-based WLSs can be precisely assessed by detailed techno-economic analysis. Herein, only the reboiler heat duty demand was estimated using the Aspen Plus®-based built-in rate-based process simulator, which implemented the proposed CO_2 solubility model and other thermophysical property models. The CO_2 absorption rate was measured using a wetted-wall column unit, and a semi-empirical model was derived and ported to the simulator (data not shown here).

The process was assumed to have a typical absorber-desorber configuration except for an absorber inter-stage cooler, with the conditions listed in Table 5. The height and diameter of the absorber/desorber were determined based on the 50% flooding condition.

Table 5. Simulation conditions of a WLS1-based CO_2 capture process.

CO_2 content (%)	15	Absorber bed height (m)	6
Flow rate of flue gas (N m^3 h^{-1})	4000	Absorber bed diameter (m)	1.31
Temp. of flue gas at the absorber inlet (K)	313	Desorber bed height (m)	1.5
Temp. of lean solvent to the absorber (K)	313	Desorber bed diameter (m)	0.65
CO_2 capture rate (%)	90	Packing material for absorber	Mellapak 500X
Min. temp. diff. in the cross HEX (K)	5	Packing material for desorber	IMTP
No. of inter-stage cooling	1	Desorber pressure	303, 505 kPa

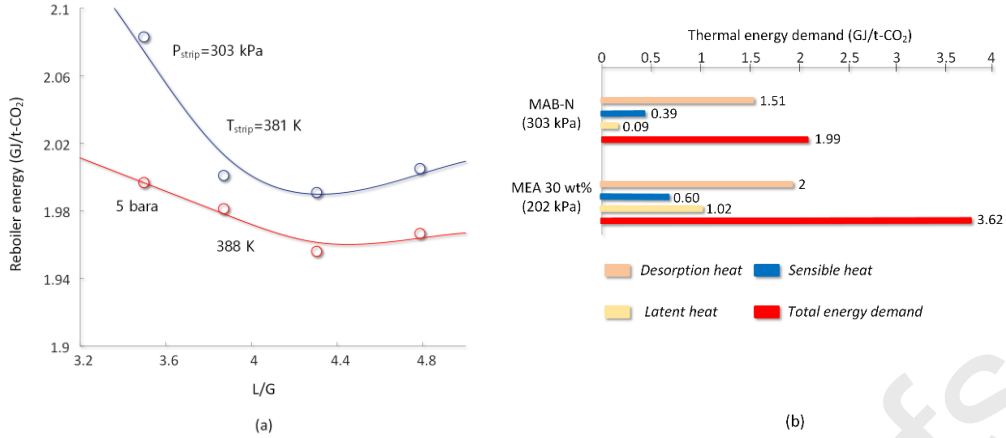

Fig. 9. (a) Total thermal energy demand of the WLS1-based process and (b) three constituents of the thermal energy demand for WLS1- and MEA 30 wt%-based processes.

Fig. 9(a) shows the thermal energy demand at the reboiler as a function of the L/G (kg-solv. kg-gas^{-1}) ratio for WLS1. The minimum thermal energy demand was estimated as 1.99 and 1.95 GJ t-CO_2^{-1} at desorber pressures of 303 and 505 kPa, respectively. The simulated thermal energy demands for WLS2 and WLS3 were only slightly different from that for WLS1 and are not shown here. In particular, the remarkably low value of reboiler heat duty, less than 2.00 GJ t-CO_2^{-1}, has not been achieved for aqueous amine solvents to the best of the authors' knowledge.

Fig. 9(b) compares the three contributors to the thermal energy demand of the WLS1-based process with those of the MEA-30 wt%-based process, revealing that all three energy terms of the former process were individually lower than those of the latter. Among them, the latent heat of water vaporization was the largest contributor to the reduction of the thermal energy demand, followed by the heat of reaction and sensible heat.

6. Conclusions

This work probes the CO_2 solubility (and other properties derived therefrom) of WLSs containing a polyamine (IBD), water, and a non-amine chemical at loadings of 60, 10–18, and 30–22 wt%, respectively.

CO_2 solubility in WLSs was modeled based on the equilibrium reactions proposed by Na *et al.* [15] , the e-NRTL model for activity representation, and the Redlich-Kwong equation of state. The Henry's law constant of CO_2 was calculated by molecular dynamics simulation. The vapor-liquid equilibrium of CO_2 and liquid-phase speciation were determined using the EC unit and $^{13}C/^{1}H$ NMR, respectively. Unknown parameters in the CO_2 solubility model were determined by fitting the experimental data to the model. The CO_2 solubility curves (isotherms) of WLSs preserved their shapes but shifted to the right with increasing water content.

The CO_2 solubility model and other property models including the CO_2 absorption rate were used to construct a process simulator using Aspen Plus®. To demonstrate the energy performance of IBD-based WLSs, we assumed a process that has a standard absorber-stripper configuration with one inter-stage cooler and treats flue gas with a CO_2 content of 15%. As a result, minimum reboiler duties of 1.99 and 1.95 GJ t-CO_2^{-1} were obtained at stripper pressures of 303 and 505 kPa, respectively, for the WLS with 10 wt% water. The corresponding reboiler temperatures at these conditions were 381 and

388 K, respectively. Itemized energy analysis comparing the case of the MEA-30 wt%-based process showed that that the largest contributor to the low reboiler duty was the latent heat of water followed by the heat of reaction and sensible heat.

Although the related data are not presented herein, the IBD-based WLSs featured excellent thermal stability, especially at low water content, and were considered to be promising energy-conservative CO_2 capture solvents worthy of further in-depth research.

Acknowledgments

This work was supported by the "Human Resources Program in Energy Technology" of the Korea Institute of Energy Technology Evaluation and Planning (KETEP) funded by the Ministry of Trade, Industry & Energy, Republic of Korea (No. 20174010201150) and the Korea CCS R&D Center (Korea CCS 2020 Project) funded by the Korean government (Ministry of Science, ICT & Future Planning) in 2017 (KCRC-2014M1A8A1049261).

References

[1] B.S. Koelbl, M.A. van den Broek, A.P. Faaij, D.P. van Vuuren, Uncertainty in Carbon Capture and Storage (CCS) deployment projections: a cross-model comparison exercise, Climatic change 123 (2014) 461-476.

[2] J. Rogelj, G. Luderer, R.C. Pietzcker, E. Kriegler, M. Schaeffer, V. Krey, K. Riahi, Energy system transformations for limiting end-of-century warming to below 1.5 C, Nature Climate Change 5 (2015) 519.

[3] M. Bui, C.S. Adjiman, A. Bardow, E.J. Anthony, A. Boston, S. Brown, P.S. Fennell, S. Fuss, A. Galindo, L.A. Hackett, Carbon capture and storage (CCS): the way forward, Energy & Environmental Science 11 (2018) 1062-1176.

[4] D. Hospital-Benito, J. Lemus, C. Moya, R. Santiago, J. Palomar, Process analysis overview of ionic liquids on CO2 chemical capture, Chemical Engineering Journal 390 (2020) 124509.

[5] W. Jung, S. Park, K.S. Lee, J.-D. Jeon, H.K. Lee, J.-H. Kim, J.S. Lee, Rapid thermal swing adsorption process in multi-beds scale with sensible heat recovery for continuous energy-efficient CO2 capture, Chemical Engineering Journal (2019) 123656.

[6] X. Zhang, Y. Huang, J. Yang, H. Gao, Y. Huang, X. Luo, Z. Liang, P. Tontiwachwuthikul, Amine-based CO2 capture aided by acid-basic bifunctional catalyst: Advancement of amine regeneration using metal modified MCM-41, Chemical Engineering Journal 383 (2020) 123077.

[7] W. Jung, J. Park, K.S. Lee, Kinetic modeling of CO2 adsorption on an amine-functionalized solid sorbent, Chemical Engineering Science 177 (2018) 122-131.

[8] M.E. Boot-Handford, J.C. Abanades, E.J. Anthony, M.J. Blunt, S. Brandani, N. Mac Dowell, J.R. Fernández, M.-C. Ferrari, R. Gross, J.P. Hallett, Carbon capture and storage update, Energy & Environmental Science 7 (2014) 130-189.

[9] D.J. Heldebrant, P.K. Koech, V.-A. Glezakou, R. Rousseau, D. Malhotra, D.C. Cantu, Water-lean solvents for post-combustion CO_2 capture: fundamentals, uncertainties, opportunities, and outlook, Chemical reviews 117 (2017) 9594-9624.

[10] D.J. Heldebrant, P.K. Koech, R. Rousseau, V.-A. Glezakou, D. Cantu, D. Malhotra, F. Zheng, G. Whyatt, C.J. Freeman, M.D. Bearden, Are water-lean solvent systems viable for post-combustion CO_2 capture?, Energy Procedia 114 (2017) 756-763.

[11] F. Barzagli, M. Di Vaira, F. Mani, M. Peruzzini, Improved Solvent Formulations for Efficient CO_2 Absorption and Low-Temperature Desorption, ChemSusChem 5 (2012) 1724-1731.

[12] P.M. Mathias, K. Afshar, F. Zheng, M.D. Bearden, C.J. Freeman, T. Andrea, P.K. Koech, I. Kutnyakov, A. Zwoster, A.R. Smith, Improving the regeneration of CO_2-binding organic liquids with a polarity change, Energy & Environmental Science 6 (2013) 2233-2242.

[13] P.M. Mathias, F. Zheng, D.J. Heldebrant, A. Zwoster, G. Whyatt, C.M. Freeman, M.D. Bearden, P. Koech, Measuring the Absorption

Rate of CO_2 in Nonaqueous CO_2-Binding Organic Liquid Solvents with a Wetted-Wall Apparatus, ChemSusChem 8 (2015) 3617-3625.

[14] M. Lail, J. Tanthana, L. Coleman, Non-aqueous solvent (NAS) CO_2 capture process, Energy Procedia 63 (2014) 580-594.

[15] S. Na, S.J. Hwang, H. Kim, I.-H. Baek, K.S. Lee, Modeling of CO_2 solubility of an aqueous polyamine solvent for CO_2 capture, Chemical Engineering Science 204 (2019) 140-150.

[16] B. Hess, C. Kutzner, D. Van Der Spoel, E. Lindahl, GROMACS 4: algorithms for highly efficient, load-balanced, and scalable molecular simulation, Journal of chemical theory and computation 4 (2008) 435-447.

[17] W.L. Jorgensen, D.S. Maxwell, J. Tirado-Rives, Development and testing of the OPLS all-atom force field on conformational energetics and properties of organic liquids, Journal of the American Chemical Society 118 (1996) 11225-11236.

[18] R.C. Rizzo, W.L. Jorgensen, OPLS all-atom model for amines: resolution of the amine hydration problem, Journal of the American Chemical Society 121 (1999) 4827-4836.

[19] H. Berendsen, J. Grigera, T. Straatsma, The missing term in effective pair potentials, Journal of Physical Chemistry 91 (1987) 6269-6271.

[20] J.G. Harris, K.H. Yung, Carbon dioxide's liquid-vapor coexistence curve and critical properties as predicted by a simple molecular model, The Journal of Physical Chemistry 99 (1995) 12021-12024.

[21] S.-N. Huang, T.A. Pascal, W.A. Goddard III, P.K. Maiti, S.-T. Lin, Absolute entropy and energy of carbon dioxide using the two-phase thermodynamic model, Journal of chemical theory and computation 7 (2011) 1893-1901.

[22] W.G. Hoover, Canonical dynamics: Equilibrium phase-space distributions, Physical review A 31 (1985) 1695.

[23] S.J. Hwang, J. Kim, H. Kim, K.S. Lee, Solubility of carbon dioxide in aqueous solutions of three secondary amines: 2-(butylamino) ethanol, 2-(isopropylamino) ethanol, and 2-(ethylamino) ethanol secondary alkanolamine solutions, Journal of Chemical & Engineering Data 62 (2017) 2428-2435.

[24] C.C. Chen, Y. Song, Generalized electrolyte-NRTL model for mixed-solvent electrolyte systems, AIChE Journal 50 (2004) 1928-1941.

[25] M.D. Hilliard, A predictive thermodynamic model for an aqueous blend of potassium carbonate, piperazine, and monoethanolamine for carbon dioxide capture from flue gas, 2008.

[26] O. Redlich, J.N. Kwong, On the thermodynamics of solutions. V. An equation of state. Fugacities of gaseous solutions, Chemical reviews 44 (1949) 233-244.

[27] C.H. Bennett, Efficient estimation of free energy differences from Monte Carlo data, Journal of Computational Physics 22 (1976) 245-268.

[28] J.M. Smith, Introduction to chemical engineering thermodynamics, ACS Publications, 1950.

[29] P.M. Mathias, J.P. O'Connell, The Gibbs–Helmholtz equation and the thermodynamic consistency of chemical absorption data, Industrial & engineering chemistry research 51 (2012) 5090-5097.

[30] R. Sander, Compilation of Henry's law constants (version 4.0) for water as solvent, Atmos. Chem. Phys 15 (2015) 4399-4981.

[31] D.M. Austgen, G.T. Rochelle, X. Peng, C.C. Chen, Model of vapor-liquid equilibria for aqueous acid gas-alkanolamine systems using the electrolyte-NRTL equation, Industrial & engineering chemistry research 28 (1989) 1060-1073.

[32] T. Edwards, G. Maurer, J. Newman, J. Prausnitz, Vapor-liquid equilibria in multicomponent aqueous solutions of volatile weak electrolytes, AIChE Journal 24 (1978) 966-976.

[33] I. Kim, H.F. Svendsen, Heat of absorption of carbon dioxide (CO_2) in monoethanolamine (MEA) and 2-(aminoethyl) ethanolamine (AEEA) solutions, Industrial & engineering chemistry research 46 (2007) 5803-5809.

Nomenclature

Acronym	
BAR	Bennett acceptance ratio
CCS	carbon capture and storage
EC	equilibrium cell
IBD	3,3'-iminobis(*N*,*N*-dimethylpropylamine)
IBDMPA	3,3'-iminobis(*N*,*N*-dimethylpropylamine)
MD	molecular dynamics
MEA	monoethanol-amine
NAC	non-amine chemical
WLS	water-lean solvent
WLS1	water-lean solvent (10 wt% of water content)
WLS2	water-lean solvent (13 wt% of water content)
WLS3	water-lean solvent (18 wt% of water content)
VLE	vapor-liquid equilibrium

Variable	
$-\Delta_{sol}A$	solvation free energy
$A_{eq,r}$	fitting parameter of the equilibrium constant
$B_{eq,r}$	fitting parameter of the equilibrium constant
$C_{eq,r}$	fitting parameter of the equilibrium constant
$D_{eq,r}$	fitting parameter of the equilibrium constant
$-\Delta_{sol}H$	solvation enthalpy
$-\Delta H_{CO2}$	heat of absorption
H	Henry's law constant
H^0	pre-exponential factor of the Henry's law constant
H_{WLS}	Henry's law constant of CO_2 in the WLS
$K_{eq,i}$	equilibrium constant of the i^{th} reaction
P	pressure
P_{CO2}	equilibrium CO_2 partial pressure
R	gas constant
T	temperature
U_{ij}	interaction energy between species *i* and *j*
a	activity
a_{ij}	fitting parameter of the binary interaction parameter
b_{ij}	fitting parameter of the binary interaction parameter

c	molar concentration
g^{ex*}	excess Gibbs free energy
$\bar{v}_M^{\infty}$	partial molar volume of CO_2 in the solution at infinite dilution
y	gas molar fraction
x	liquid molar fraction
Greek	
α_{CO2}	CO_2 loading
ϕ	fugacity coefficient
σ	normalization factor
γ	activity coefficient
η	stoichiometric coefficient
τ_{ij}	binary interaction parameter

Supporting Information

Table S1. Solubility of CO_2 in WLSs.

WLS1: IBD : NAC : water = 60 : 30 : 10 w/w/w								
T (K)	mol mol^{-1}	P_{CO2} (kPa)	T (K)	mol mol^{-1}	P_{CO2} (kPa)	T (K)	mol mol^{-1}	P_{CO2} (kPa)
313	0.10	0.49	353	0.09	21.62	373	0.04	55.84
	0.23	1.93		0.13	36.61		0.07	87.30
	0.31	3.63		0.18	55.62		0.10	120.74
	0.43	12.78		0.25	81.27		0.13	160.11
	0.53	27.39		0.30	114.74		0.17	229.12
	0.65	66.54		0.35	153.68		0.21	281.38
	0.74	110.33		0.39	202.36		0.25	340.46
333	0.07	2.30		0.46	283.07		0.29	437.12
	0.10	3.82		0.54	337.05	393	0.0071	104.37
	0.14	6.16		0.59	418.28		0.042	206.86
	0.21	11.70					0.081	340.25
	0.26	15.37					0.10	417.21
	0.30	19.59						
	0.36	31.62						
	0.44	55.99						
	0.54	104.54						

WLS2, IBD : NAC : water = 60 : 27 : 13 w/w/w								
T (K)	mol mol^{-1}	P_{CO2} (kPa)	T (K)	mol mol^{-1}	P_{CO2} (kPa)	T (K)	mol mol^{-1}	P_{CO2} (kPa)
313	0.17	0.50	353	0.05	6.48	373	0.10	85.78
	0.23	0.96		0.10	16.96		0.15	134.90
	0.33	2.56		0.16	27.26		0.23	219.25
	0.50	13.02		0.21	48.63		0.28	294.12
	0.60	26.87		0.27	64.43		0.35	367.93
	0.67	44.79		0.32	88.81	393	0.050	98.42
	0.74	66.28		0.36	117.44		0.095	185.34
333	0.14	4.27		0.43	167.67		0.13	255.05
	0.21	8.09					0.15	314.68
	0.28	13.68						
	0.35	23.08						
	0.41	36.13						
	0.48	57.58						

WLS3, IBD : NAC : water = 60 : 22 : 18 w/w/w								
T (K)	mol mol^{-1}	P_{CO2} (kPa)	T (K)	mol mol^{-1}	P_{CO2} (kPa)	T (K)	mol mol^{-1}	P_{CO2} (kPa)
313	0.17	0.20	353	0.13	15.14	373	0.087	50.96
	0.27	0.61		0.23	32.98		0.20	136.78
	0.37	1.64		0.33	60.40		0.24	176.05
	0.46	4.08		0.40	108.49		0.30	272.51
	0.56	10.83		0.51	173.64		0.37	344.14
	0.66	22.79		0.59	263.24	393	0.043	100.16
	0.78	47.25					0.076	169.77
	0.91	80.39					0.11	238.09
333	0.17	2.81					0.13	310.60
	0.27	7.00						
	0.37	14.30						
	0.47	34.24						
	0.55	53.45						
	0.64	93.10						
	0.72	142.08						

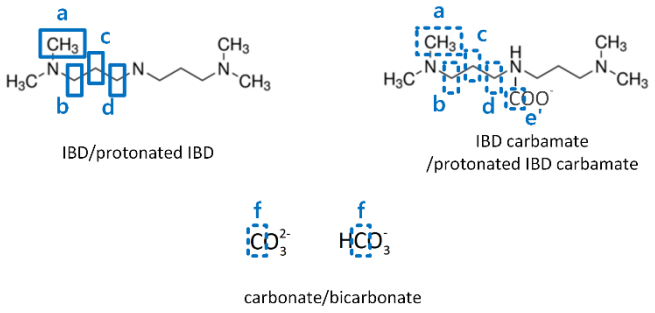

Fig. S1. Functional groups of (protonated) IBD, (protonated) IBD carbamate, and (bi)carbonate.

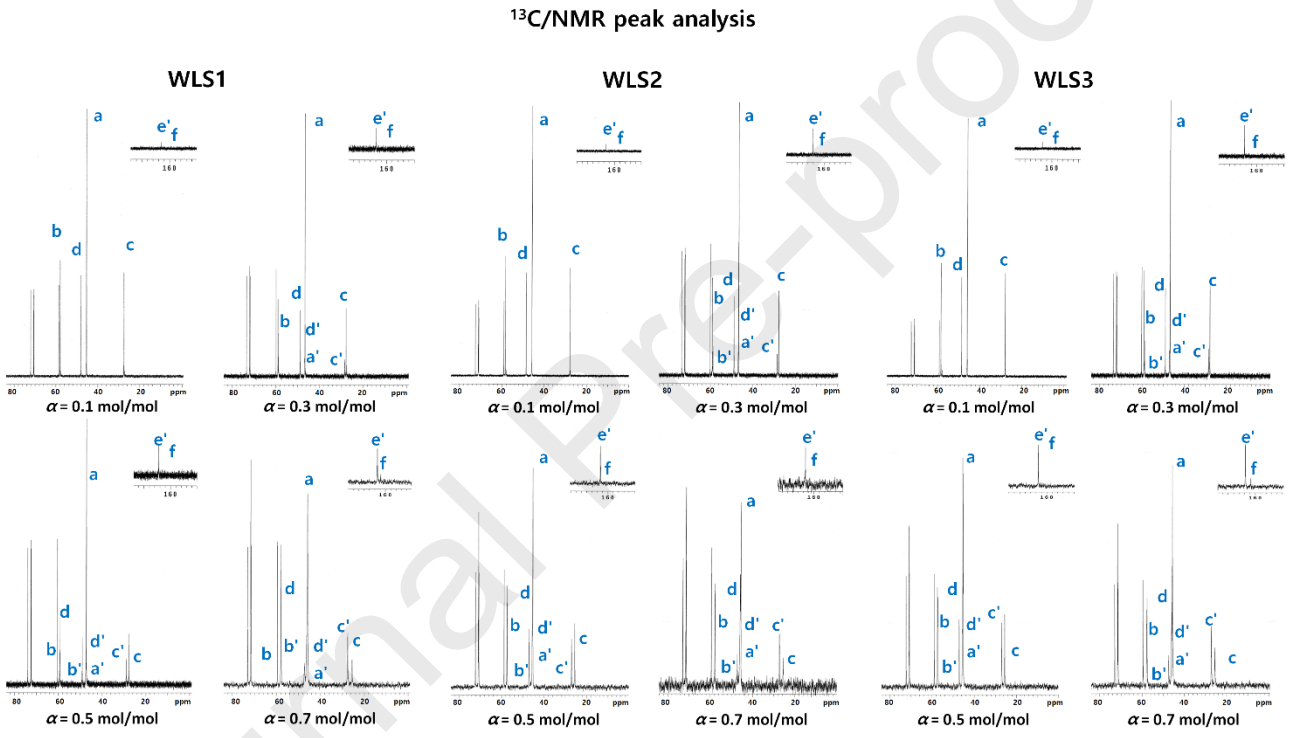

(a)

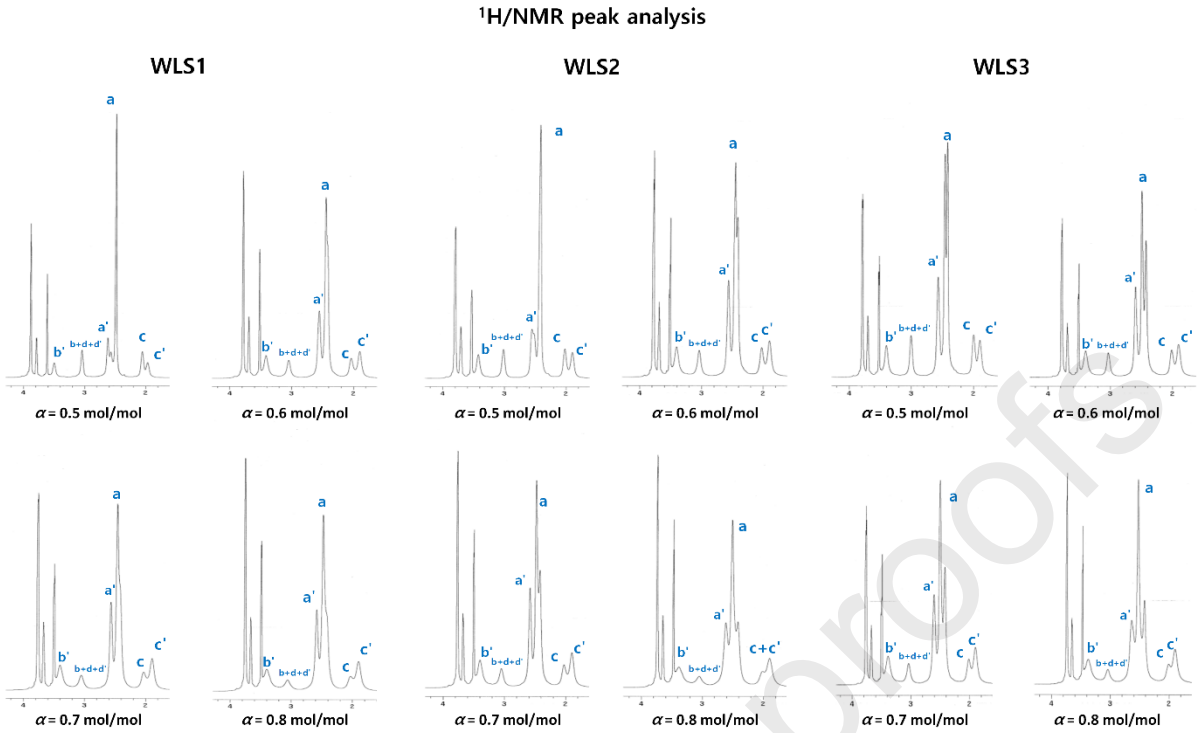

(b)

Fig. S2. (a) ^{13}C NMR data (with assignments based on the code in Fig. S1) for WLS1–3 at CO_2 loadings of α = 0.1, 0.3, 0.5, and 0.7 mol mol^{-1}. (b) ^{1}H NMR data for WLS1–3 at CO_2 loadings of α = 0.5, 0.6, 0.7, and 0.8 mol mol^{-1}. The exact shifts are listed in Table S2.

Table S2. Chemical shifts of WLSs.

Peak	Functional group	^{13}C NMR δ (ppm)	^{1}H NMR δ (ppm)
a	CH_3–N–	43.738	1.954
b	–CH_2–N–	56.087	2.356
c	–CH_2–	25.431	1.429
d	–CH_2–NH-	46.486	2.126
a'	CH_3–N–	43.458	2.058
b'	–CH_2–N–	55.553	2.931
c'	–CH_2–	24.956	1.449
d'	–CH_2–NH–	44.191	2.202
e'	COO^-	163.414	Not available
f	CO_3^{2-}/HCO_3^{2-}	164.905	Not available

Declaration of interests

☒ The authors declare that they have no known competing financial interests or personal relationships that could have appeared to influence the work reported in this paper.

☐The authors declare the following financial interests/personal relationships which may be considered as potential competing interests:

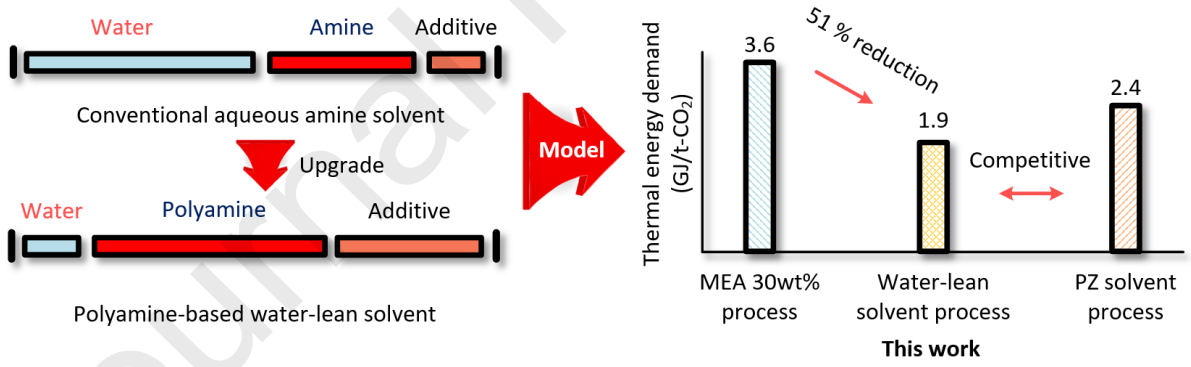

Highlights

- Absorption-based CO_2 capture process with polyamine-based water-lean solvent was proposed.
- Thermodynamic model of the proposed water-lean solvent was developed by measuring CO_2 vapor-liquid equilibrium.
- Henry's law constant was estimated by using molecular dynamics simulation.

- The energy performance of proposed water-lean solvent process was evaluated by experiments and modeling.